# Viscous Sublayer Below a Wind-Disturbed Water Surface

JIN WU

*Air–Sea Interaction Laboratory, College of Marine Studies, University of Delaware, Lewes, DE 19958*

(Manuscript received 27 June 1983, in final form 26 September 1983)

ABSTRACT

Drift currents immediately below the water surface were systematically measured in a circulating wind-wave tank. The results confirmed the existence of a viscous sublayer at the air–water interface, with the current varying linearly with depth and the shear stress determined from the linear profile comparing very favorably with the wind stress. The thickness ($\delta_v$) of the sublayer was found to be almost invariant with wind velocity. Its nondimensional thickness ($\delta_v u_*/\nu$) is smaller than that over a solid surface, having a value of 4 at low wind velocities and increasing with wind velocity toward the solid-surface value of 8 at high wind velocities.

## 1. Introduction

The aqueous boundary layer of the upper ocean is generally turbulent (Grant *et al.*, 1968). Due to the damping of turbulence by the air–sea interface, a viscous region has been considered to exist immediately below the sea surface, and to provide a vital link between air and sea systems. This region, the so-called viscous sublayer, is very thin and may be temporarily disrupted by breaking waves. Near the upper boundary of the viscous region, a thermal sublayer governs heat exchange between the atmosphere and the ocean (Ewing and McAlister, 1960; Roll, 1965), and a diffusion sublayer provides the main resistance to gas transfer through the sea surface (Deacon, 1977). Understanding of the structure of the viscous sublayer, therefore, is also a prerequisite for studying heat and gas transfers across the air–sea interface.

Exploratory measurements of Wu (1975) and McLeish and Putland (1975) illustrated the existence of a region within which the current varied linearly with depth, and hinted that this region might be thinner than the viscous sublayer over a solid surface. In the meantime, the consideration of molecular processes governing heat transfer near the sea surface was substantiated among others by McAlister and McLeish (1969) and Khundzhua *et al.* (1977). The thicknesses of the viscous and thermal sublayers below the water surface were also estimated (Wu, 1971) by considering that the aqueous boundary layer below the interface behaves similarly as a hydrodynamically smooth boundary layer over a solid surface. Such a similarity, however, may be influenced by drifting motions of the interface (Saunders, 1973) and the presence of surface waves (Csanady, 1978).

Systematic measurements of currents immediately below the air–water interface have been performed in a specially designed tank. Without breaking waves, the velocity distribution and the shear stress within a thin region were verified to follow those of the viscous sublayer. The thickness of this region, the viscous sublayer, was found to be invariant with wind velocity and to be generally thinner than that over a solid surface. Expressions are proposed for the non-dimensional thickness of the viscous sublayer below the water surface in hydrodynamically smooth flows, having a value of 4 at low wind velocities and increasing toward but not exceeding the solid-surface value of 8 at high wind velocities.

## 2. Previous experiments

### a. Measurements

Airflows above and drift currents below the air–water interface under various wind conditions were systematically measured by Wu (1975). Transitions of the current boundary layer to various regimes were found to occur at higher wind velocities than those of the airflow boundary layer. The drift currents immediately below the air–water interface, measured with surface floats, varied approximately linearly with depth. It appears that the turbulence within this thin layer, heaving up and down with surface waves, is damped by the solidity (nonpenetration by eddies) of the interface. This is the so-called viscous sublayer, which can be disrupted only temporarily when waves break. Assuming that the viscous sublayer has the same thickness as that over a solid boundary (Schlichting, 1968), the shear stress determined from a linear velocity distribution fitted to the data within this assumed region was found to be smaller than that calculated from the logarithmic velocity distribution away from the interface. This appears to suggest that the sublayer near the air–water interface is thinner than that over a solid surface; because the velocity gradient is greater within

than outside the sublayer, a smaller shear stress is therefore indicated by the linear profile fitted to a region extending beyond the sublayer.

McLeish and Putland (1975) performed measurements with microscopic bubbles that were produced by a pulsating electrical current through a fine wire supported vertically in a small wind–wave tank. Their results consist of only a single current profile determined from photographs of displaced bubble lines. The linear region of the profile was found to be only about one third the corresponding viscous-sublayer thickness over a solid surface.

*b. Comments*

Spherical floats were used by Wu (1975) to measure currents immediately below the water surface. Although an approximately linear variation of current with depth was detected with these floats, the major purpose of that portion of his experiments was to determine the surface drift from the vertical distribution of measured currents. Neither geometrical shape nor size of the floats was appropriate for tracing accurately currents within the sublayer.

McLeish and Putland's (1975) lone current profile was obtained at a rather low wind velocity. Besides having difficulty in locating the undulating water surface, their results were perhaps affected by the rising of bubbles. Although, as they reported, the rising velocity of an individual bubble is only about 0.6 mm $s^{-1}$, a line of densely crowded bubbles should rise much faster than this rate.

In summary, previous studies on the viscous sublayer at the air–water interface appear to be deficient because of their experimental technique. Moreover, their measurements were limited to the shape of the velocity profile not concerned with the shear stress. Nonetheless, there were indications that the sublayer at the air–water interface may behave differently from that over solid surface. More careful experiments over varied wind and wave conditions must be conducted first to verify the existence of the viscous sublayer at the interface by including the measurement of shear stress, and then to determine the functional variation of the sublayer thickness with wind velocity.

## 3. Present measurements

*a. Experiments*

1) TANK

The experiments have been conducted in a tank, which has the shape of a race track; see Fig. 1. The tank has two straight sections each 350 cm long, and two semicircular sections with a center-line radius of 185 cm; the width of the tank is 31 cm with a 15.5 cm high wind tunnel above water 31 cm deep. An impeller driven by a variable speed motor was installed in a Ω-shaped duct along the straight stretch in the back. As shown in the figure, horizontal guiding vanes were placed on both sides of the impeller for a smooth transition of the airflow. Vertical guiding vanes of wind and currents as shown in the figure were installed in the curved sections to suppress secondary spiral motions around the bend. The straight stretch in the front is the test section. Negligible disturbances were introduced by the vertical guiding vanes; the flows were found to be uniform across the tank at about one tank width downwind from the end of the vanes. The velocity within the wind tunnel can be varied up to 9 m $s^{-1}$.

This circulating tank was designed to avoid end effects presented in a straight tank, which induce upwind currents near the tank bottom. These return currents may affect the structure of the aqueous boundary layer. Another shortcoming of the straight tank is that the wave structure, and consequently the wind stress, vary significantly along the tank. In the present setup, however, both wind and wave structures reach equilibrium states shortly after the wind has been turned on, and subsequently vary little along the tank. Furthermore, a large portion of energy supplied by the wind is consumed on wave generation in a straight tank (Stewart, 1961; Wu, 1973), where waves are damped on the beach at the downwind end. Such artificial effects, leaving only a portion of the momentum flux from wind for producing currents (Lighthill, 1971), were largely eliminated in the present endless tank, where waves propagate along the tank without much damping. This makes it more certain to relate measured aqueous flows to the wind stress.

2) WIND CONDITIONS

For each wind condition, velocity profiles were measured at three stations, 1 m apart, along the middle reach of the test section. The wind velocity was verified to follow the Karman–Prandtl distribution (Wu, 1968).

$$\frac{u_a}{u_{*a}} = \frac{1}{\kappa} \ln\left(\frac{z}{z_{0a}}\right), \tag{1}$$

in which $u_a$ is the velocity at the elevation $z$ above the mean water surface, $u_{*a} = (\tau_a/\rho_a)^{1/2}$ the wind-friction velocity with $\tau_a$ being the wind stress and $\rho_a$ the air density, $\kappa = 0.4$ the Karman constant, and $z_{0a}$ the roughness length. The friction velocity and roughness length determined from the wind profile are presented in Fig. 2a, b, where $U_a$ is the maximum wind velocity in the tunnel. The trends of the results seen in the figure are typical for those obtained at low wind velocities (Wu, 1968, 1975), where the wind–wave interaction is in the surface-tension governing regime. Both the roughness length and the wind-stress coefficient in this regime have been shown to decrease as the wind velocity increases (Wu, 1968).

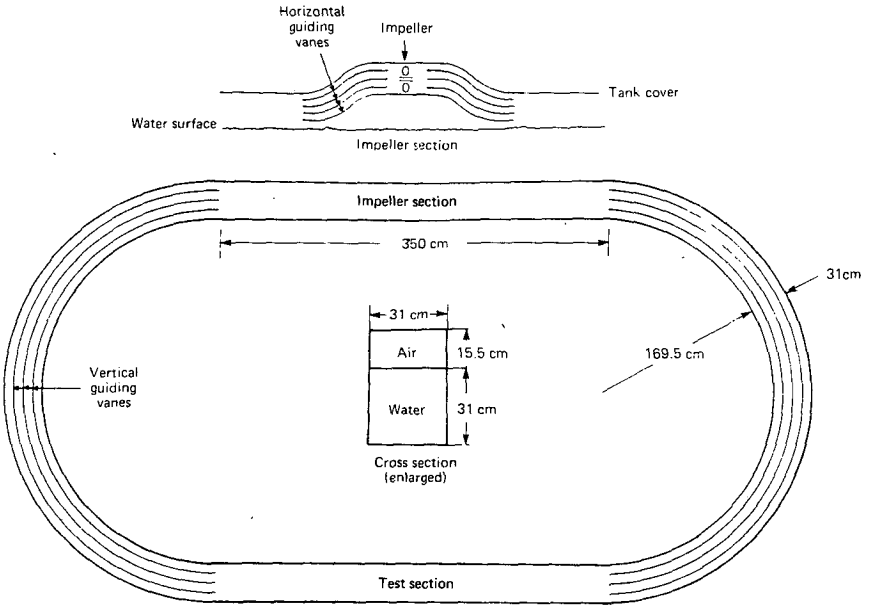


FIG. 1. Circulating wind-wave tank.

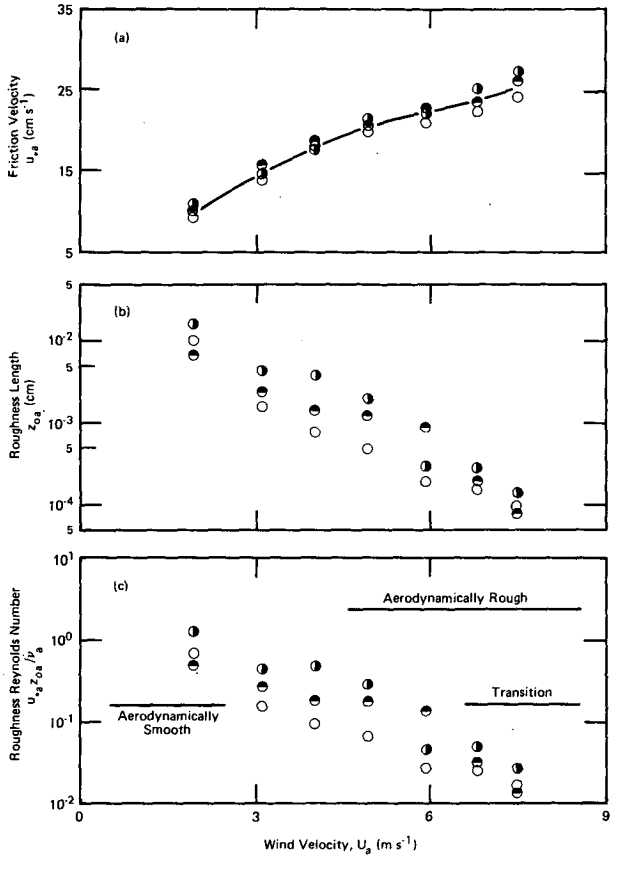


FIG. 2. (a) Friction velocities, (b) roughness lengths, and (c) roughness Reynolds numbers. The symbols correspond to the locations marked the beginning (○), middle (◒), and end (◑) of the reach for current measurements.

The roughness Reynolds numbers, $u_{*a}z_{0a}/\nu_a$ (where $\nu_a$ is the kinematic viscosity of air), can now be calculated and are shown in Fig. 2c along with the critical roughness Reynolds numbers identifying various flow regimes (Schlichting, 1968). The results indicate that the airflow boundary layer in the present facility is aerodynamically smooth. This further indicates that the aqueous boundary should be hydrodynamically smooth, as the transition to various boundary layer regimes always occur at higher wind velocities on the water side than on the air side (Wu, 1973, 1975). When the wind velocity in the tank reached 8 m s$^{-1}$, waves started to break, disrupting the sublayer. A rather long restoration time, generally in the neighborhood of 10 seconds (Ewing and McAlister, 1960), made measurements of the sublayer futile.

### 3) CURRENT MEASUREMENTS

It is very hard, if it is not impossible, to let a velocity probe follow the undulating water surface with an accuracy, say of a tenth of a millimeter, necessary for measuring currents within the sublayer. Consequently, instead of an Eulerian-type probe, a Langragian-type tracer, spherical particles in the earlier experiment (Wu, 1975) and cylindrical discs in the present experiment, were used. Interpretation of the current indicated by discs in a flow field with a steep velocity gradient is more certain than that indicated by particles. Discs of various sizes, 2–5 mm in diameter and 0.1–5 mm in thickness, were used. Generally, discs having smaller diameters but still being able to maintain its orientation with their cylindrical axis normal to the water surface during the test were chosen. These floats were nearly

neutrally buoyant with a negligible protrusion above the water surface to minimize the wind drag. The submergence of the float was calculated from its weight and dimension. The floats were timed between two stations 1 m apart in the middle reach of the test section. More than twenty timings were taken for each float, and the velocity averaged from these readings was considered as the current at a depth one half the float's submergence. From measurements with surface floats of various submergences, the vertical distribution of currents was obtained.

*b. Results*

1) CURRENT DISTRIBUTION

Currents measured with discs under different wind velocities are shown in Fig. 3, where $u$ is the current at the depth $z$ below the (undulating) water surface. Among floats of various dimensions no influence of diameter on measured currents was found for thin discs, while for thick discs currents measured with those having larger diameters appeared to be slightly greater. The data obtained with discs having a diameter larger than 4 mm were excluded from Fig. 3. It is seen in the figure that the current immediately below the water surface varies linearly with depth and that the region with a linear current profile can be clearly identified. The current in this region, the viscous sublayer, is therefore fitted with a straight line. Outside the sublayer, the gradient of currents is much smaller, and the current distribution is indicated by a curve.

2) SHEAR STRESS

The shear stress of currents can be determined from the slope of the straight line shown in Fig. 3,

$$\tau = \mu \frac{d(u_s - u)}{dz}, \tag{2}$$

where $\tau$ is the shear stress, $\mu$ the dynamic viscosity of water and $u_s$ the surface current determined by extending the fitted straight line to the water surface. The friction velocity of the currents can be determined from $u_* = (\tau/\rho)^{1/2}$, where $\rho$ is the density of water.

From the reference wind velocity ($U_a$) shown in Fig. 3, the corresponding friction velocity of the wind can be found from the curve faired to the data shown in Fig. 2a. The ratio between the shear stress acting on the underside of the interface ($\rho u_*^2$) and that on the upperside ($\rho_a u_{*a}^2$) can now be determined, and is presented in Fig. 4. The results can be represented very closely by $\rho u_*^2/\rho_a u_{*a}^2 = 0.95$, shown as a straight line in the figure. As pointed out earlier, waves propagating around the present endless tank have negligible damp-

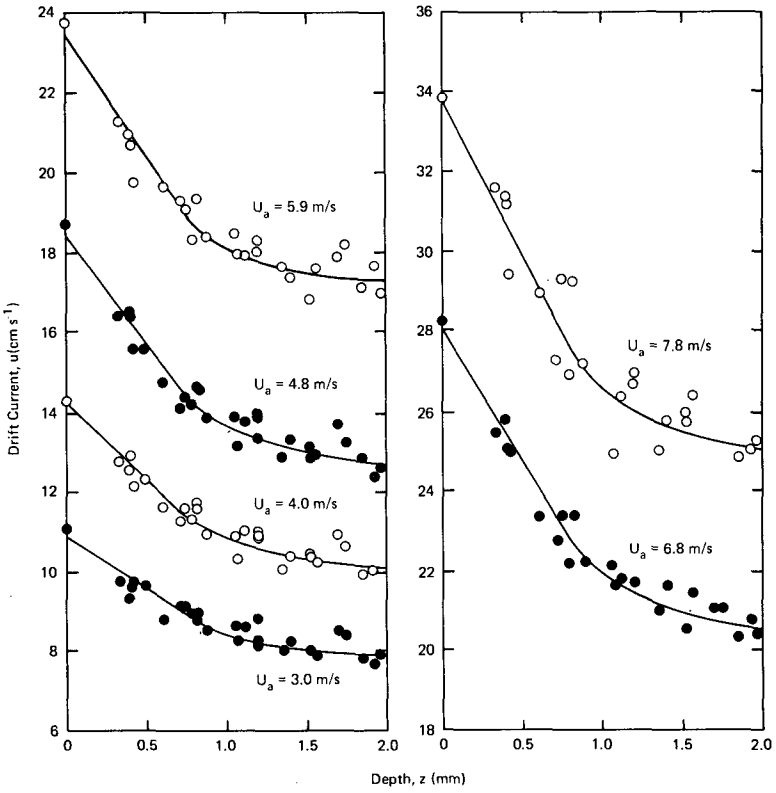


FIG. 3. Vertical distributions of currents measured with disc floats.

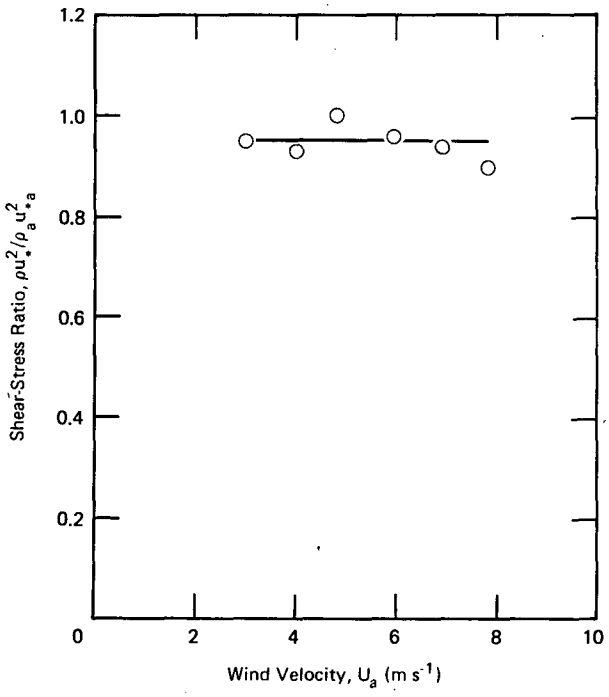


FIG. 4. Ratios between shear stresses acting on under- and upper-sides of air–water interface.

ing; consequently, the ratio shown in Fig. 4 has a value of very nearly unity. This makes the present tank, as discussed earlier, more suitable than a straight tank for studying the aqueous boundary layer.

The shear stress determined from the linear profile is compared here with the wind stress rather than with the shear stress determined from the logarithmic current profile as in Wu (1975). The former comparison is on a more solid ground than the latter; as pointed out by Csanady (1978), there are a number of uncertainties concerning the numerical values of coefficients and constants in the logarithmic distribution.

### 3) SUBLAYER THICKNESS

The non-dimensional thickness of the viscous sublayer over a solid surface was found (Schlichting, 1968) to remain invariant as

$$\delta_v^+ = \frac{\delta_v u_*}{\nu} = 8, \tag{3}$$

where $\delta_v$ and $\delta_v^+$ are the physical and the nondimensional thicknesses of the viscous sublayer, and $\nu$ is the kinematic viscosity of water. According to this expression, the thickness of the viscous sublayer over the solid boundary varied inversely with the friction velocity. The nominal nondimensional thickness of the viscous sublayer is 11.6 where the linear velocity profile intersects the logarithmic profile. The velocity, however, deviates noticeably from the linear profile at about ⅔ of this value.

The physical thickness of the viscous sublayer over the air–water interface, determined from the lower end of the straight line shown in Fig. 3, is presented in Fig. 5a. An almost constant thickness, $\delta_v = 0.8$ mm, is seen in the figure except at the lowest wind velocity. Consequently, for most wind velocities the nondimensional thickness of the viscous sublayer over the air-water interface, instead of having a constant value, increases with the friction velocity as illustrated in Fig. 5b. Overall, the nondimensional thickness of the viscous sublayer over the air–water interface is seen in the figure to be thinner than that over a solid surface. At the low-wind-velocity end, the nondimensional thickness appears to approach asymptotically $\delta_v^+ = 4$. We do not have sufficient data to determine whether the thickness of the viscous sublayer increases continuously with the friction velocity even beyond $\delta_v^+ = 8$. However, the results shown in Fig. 5b have already indicated that the viscous sublayer over the air-water interface is thinner than that over a solid surface. Consequently, as long as the aqueous boundary layer is hydrodynamically smooth it is very unlikely that the nondimensional thickness of the viscous sublayer would exceed the solid-surface value at high friction velocities. Accepting this argument and the asymptotic value at the lowest wind velocity, the following expressions are suggested

$$\left.\begin{aligned} &\delta_v^+ = 4, \quad u_* < 0.2 \text{ cm s}^{-1} \\ &\delta_v^+ = 4 + 6.3(u_* - 0.2)^2, \\ &\quad 0.2 \text{ cm s}^{-1} \leqslant u_* \leqslant 1.0 \text{ cm s}^{-1} \\ &\delta_v^+ = 8, \quad u_* > 1.0 \text{ cm s}^{-1} \end{aligned}\right\}, \tag{4}$$

where $u_*$ is expressed in cm s$^{-1}$; these expressions are illustrated in Fig. 5b. In summary, unlike that over a solid surface, the non-dimensional thickness of the viscous sublayer over the air–water interface varies with currents.

## 4. Discussion

### *a. Other investigations*

The viscous sublayer has scarcely been studied. A single current profile at a rather low wind velocity, as discussed previously, was measured by McLeish and Putland (1975). Both the thickness and the friction velocity can be obtained from their current profile; subsequently, we can determine the nondimensional thickness of the viscous sublayer in their experiment as $\delta_v^+ = 4$ at $u_* = 0.65$ cm s$^{-1}$. This, first of all, is indeed smaller than the solid-surface value, and is also in fair agreement with $\delta_v^+ = 5.2$ calculated from the present model.

There is only one set of direct measurements of the thermal sublayer. Using a miniature thermocouple, Khundzhua *et al.* (1977) measured the temperature profile immediately below the sea surface, and found

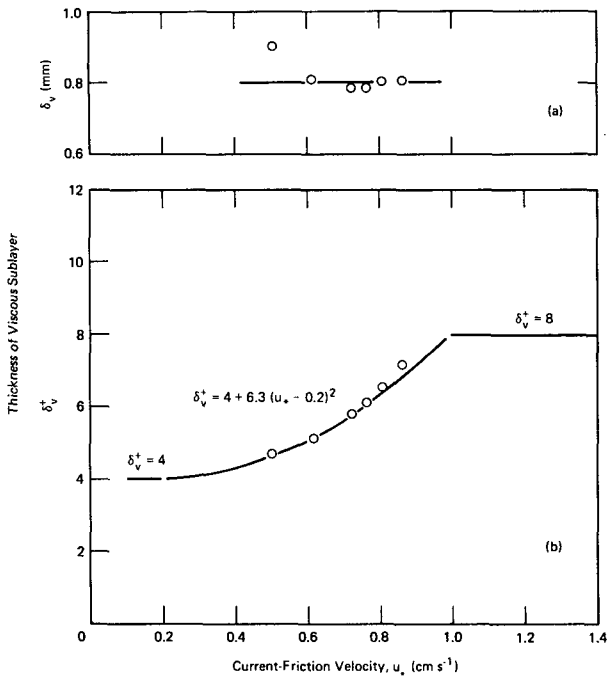


FIG. 5. (a) Physical and (b) nondimensional variations of thicknesses of viscous sublayer with friction velocity.

the thickness of the thermal sublayer to be 0.2–0.6 mm for wind velocities 6–8 m s$^{-1}$. Averaging both values, we have the thickness of the thermal sublayer $\delta_t = 0.3$ mm at $U = 7$ m s$^{-1}$. For this wind velocity, the wind-friction velocity can be obtained from the formula of wind stress coefficients suggested by Wu (1980) as $u_{*_a} = 24.8$ cm s$^{-1}$. Subsequently, the friction velocity of currents can be estimated as $u_* = (\rho_a/\rho)^{1/2} u_{*_a} = 0.84$ cm s$^{-1}$. Considering the difference between the dynamic viscosity and the heat conductivity of sea water, the thermal sublayer was suggested to be one half as thick as the viscous sublayer (Wu, 1971), $\delta_v = 2\delta_t$. Consequently, we have for the measurements of Khundzhua *et al.* $\delta_v^+ = 5.2$. The latter is again smaller than the solid-surface value, and also compared favorably with the value calculated from Eq. (4), $\delta_v^+ = 6.6$.

### *b. Proposed expressions*

The existence of a viscous sublayer, as discussed previously, is due to the damping of turbulence at the boundary, where fluid motions vanish. At the air–water interface the boundary not only moves longitudinally in the wind direction, but also undulates vertically. Assessing primarily horizontal motions at the interface in contrast to nonslip conditions at the solid surface, Saunders (1973) suggested that turbulent processes should penetrate closer to the boundary in the former case than in the latter case. We would further suggest that vertical surface undulations, with frequencies comparable with those of turbulence, should also make the flow near the air–water interface less stable than that over a fixed boundary, again implying that turbulence penetrates closer to the interface than to a solid surface. Therefore, the viscous sublayer at the interface is thinner than that at a solid surface, as illustrated by the overall trend shown in Fig. 5b.

The thinning of the sublayer due to characteristic features of the air–water interface—longitudinal motions and vertical undulations—should be relatively more effective at lower wind velocities, where the sublayer is relatively thick. Consequently, in comparison with that over the solid surface, the sublayer at the interface is thinner at higher wind velocities and much thinner at lower wind velocities. In other words, unlike at a solid surface where the sublayer thickness decreases with increasing fluid velocity, the sublayer at the air–water interface tends to maintain a constant thickness, as illustrated by the results shown in Fig. 5a.

As wind velocity decreases, turbulence becomes less pronounced. Consequently, the nondimensional thickness of the viscous sublayer cannot decrease continuously with wind velocity; a lower limit should soon be reached, with the nondimensional thickness reaching an asymptotic value. On the other hand, the thinning effects due to interfacial characteristics diminish when the sublayer becomes thinner at higher wind velocities; we see that at a certain wind velocity these effects become insignificant when the sublayer is very thin. In other words, the nondimensional thickness cannot increase continuously with the wind velocity on the high-wind-velocity end. Inasmuch as the thickness of the viscous sublayer over the air–water interface should be thinner than that over a solid surface, the nondimensional thickness for a solid surface is adopted as the upper limit.

## 5. Concluding remarks

The viscous sublayer over the air–water interface appears to behave differently from that over a solid surface. It is thinner at low wind velocities, and approaches the solid-surface value at high wind velocities. The present results are consistent with those of other observations. The present study, however, is limited to hydrodynamically smooth flows. As for hydrodynamically rough flows, besides different flow structures over both surfaces, the problem is further complicated by different behaviors of roughness elements in the two cases, not to mention the difficulty involved in identifying these elements for the air–water interface (Wu, 1975). The concept of effective viscosity was advanced by Csanady (1978) for the law of the wall of turbulent flows along a density interface (Lofquist, 1960). The effective viscosity incorporates the basic molecular effect with the wave influence. The present results show that within the viscous sublayer at the air-water interface the molecular viscosity is sufficient to relate the velocity gradient to shear stress.

*Acknowledgment.* I am very grateful for the sponsorship of this work provided by the Mechanics Division, Office of Naval Research, under Contract N00014-83-K-0316 and the Physical Oceanography Program, National Science Foundation, under Grant OCE-8214998.

## REFERENCES

Csanady, G. T., 1978: Turbulent interface layers. *J. Geophys. Res.*, **83,** 2329–2342.

Deacon, E. L., 1977: Gas transfer to and across an air–water interface. *Tellus,* **29,** 363–374.

Ewing, G., and E. D. McAlister, 1960: On the thermal boundary of the ocean. *Science,* **131,** 1374–1376.

Grant, H. L., A. Moilliet and W. M. Vogel, 1968: Some observations of the occurrence of turbulence in and above thermocline. *J. Fluid Mech.*, **34,** 443–448.

Khundzhua, G. G., A. M. Gusev, Ye. G. Andreyev, V. V. Gurov and N. A. Skorokhvatov, 1977: Structure of the cold surface film of the ocean and heat transfer between the ocean and the atmosphere. *Izv. Acad. Sci. USSR Atmos. Oceanic Phys.*, **13,** 506–509.

Lighthill, M. J., 1971: Time-varying currents. *Phil. Trans. Roy. Soc. London,* **A271,** 371–390.

Lofquist, K., 1960: Flow and stress near an interface between stratified liquids. *Phys. Fluids,* **3,** 158–175.

McAlister, E. D., and W. McLeish, 1969: Heat transfer in the top millimeter of the ocean. *J. Geophys. Res.*, **74,** 3408–3414.

McLeish, W., and G. E. Putland, 1975: Measurements of wind-driven flow profiles in the top millimeter of water. *J. Phys. Oceanogr.*, **5,** 516–518.

Roll, H. U., 1965: *Physics of the Marine Atmosphere.* Academic Press, 426 pp.

Saunders, P. M., 1973: The skin temperature of the ocean, a review. *Mém. Soc. R. Sci. Liège 6e Ser.*, **6,** 93–98.

Schlichting, H., 1968: *Boundary-Layer Theory.* McGraw-Hill, 747 pp.

Stewart, R. W., 1961: The wave drag of wind over water. *J. Fluid Mech.*, **10,** 189–194.

Wu, Jin, 1968: Laboratory studies of wind–wave interaction. *J. Fluid Mech.*, **34,** 91–112.

——, 1971: An estimation of oceanic thermal-sublayer thickness. *J. Phys. Oceanogr.*, **1,** 284–286.

——, 1973: Wind-induced turbulent entrainment across a stable density interface. *J. Fluid Mech.*, **61,** 275–287.

——, 1975: Wind-induced drift currents. *J. Fluid Mech.*, **68,** 49–70.

——, 1980: Wind-stress coefficients over sea surface near neutral conditions—a revisit. *J. Phys. Oceanogr.*, **10,** 727–740.